Comput. Methods Appl. Mech. Engrg. 200 (2011) 1237–1250

Contents lists available at ScienceDirect

Comput. Methods Appl. Mech. Engrg.

journal homepage: www.elsevier.com/locate/cma

# Continuous and discontinuous finite element methods for a peridynamics model of mechanics ☆

X. Chen, Max Gunzburger *

*Department of Scientific Computing, Florida State University, Tallahassee, FL 32306-4120, USA*

ARTICLE INFO

*Article history:*
Received 4 March 2010
Received in revised form 27 September 2010
Accepted 11 October 2010
Available online 27 October 2010

*Keywords:*
Peridynamics
Discontinuous Galerkin methods
Finite element methods

ABSTRACT

In contrast to classical partial differential equation models, the recently developed peridynamic nonlocal continuum model for solid mechanics is an integro-differential equation that does not involve spatial derivatives of the displacement field. As a result, the peridynamic model admits solutions having jump discontinuities so that it has been successfully applied to fracture problems. The peridynamic model features a horizon which is a length scale that determines the extent of the nonlocal interactions. Based on a variational formulation, continuous and discontinuous Galerkin finite element methods are developed for the peridynamic model. Discontinuous discretizations are conforming for the model without the need to account for fluxes across element edges. Through a series of simple, one-dimensional computational experiments, we investigate the convergence behavior of the finite element approximations and compare the results with theoretical estimates. One issue addressed is the effect of the relative sizes of the horizon and the grid. For problems with smooth solutions, we find that continuous and discontinuous piecewise-linear approximations result in the same accuracy as that obtained by continuous piecewise-linear approximations for classical models. Piecewise-constant approximations are less robust and require the grid size to be small with respect to the horizon. We then study problems having solutions containing jump discontinuities for which we find that continuous approximations are not appropriate whereas discontinuous approximations can result in the same convergence behavior as that seen for smooth solutions. In case a grid point is placed at the locations of the jump discontinuities, such results are directly obtained. In the general case, we show that such results can be obtained through a simple, automated, abrupt, local refinement of elements containing the discontinuity. In order to reduce the number of degrees of freedom while preserving accuracy, we also briefly consider a hybrid discretization which combines continuous discretizations in regions where the solution is smooth with discontinuous discretizations in small regions surrounding the jump discontinuities.



## 1. Introduction

Nonlocal theories in continuum mechanics have been introduced since at least the 1970s [17,18,23] and have recently become topical again [1–3,7,19,21,22,24,33,34]. The *peridynamics* model [24,30] is one such nonlocal theory formulated to describe the formation of discontinuities, e.g., cracks and fractures due to deformations, in the displacement field. In contrast to the classical local theory and also to most other nonlocal approaches, the peridynamic equation of motion is free of any spatial derivatives of the displacement. The peridynamic model has been applied in several settings; see, e.g., [4–6,14,15,25,27–29]. Modeling and theoretical studies regarding the peridynamic model are found in, e.g., [8,9,11,16,24,26,30–32,35–39] whereas its computational solution is considered in, e.g., [6,11,13–15,20,28,36,37]. In particular, finite element discretizations are considered in [13,20,37].

In this paper, we study the use of continuous and discontinuous Galerkin finite element methods for discretizing a specific linear peridynamics model. We study the performance of straightforward finite element discretizations, showing that they fail to adequately treat problems having discontinuous solutions. We show, using an one-dimensional setting, that several variants of the straightforward approaches that naturally suggest themselves do not completely ameliorate the inadequacies of the latter. We then develop a finite element method that uses local refinement and that obtains the same optimal convergence rates for problems having solutions containing jump discontinuities as it does for problems having smooth solutions. We note that previous studies of finite element methods for the peridynamics model [13,20,37] do not consider the same issues, and in fact, deal with problems

☆ This work was supported by the US Department of Energy under Grant Numbers DE-FG02-05ER25698 and DE-SC0004970 and by the US Air Force Office of Scientific Research under Grant Number FA9550-08-1-0415.

* Corresponding author.
*E-mail addresses:* xc07@fsu.edu (X. Chen), gunzburg@fsu.edu (M. Gunzburger).

0045-7825/$ - see front matter © 2010 Elsevier B.V. All rights reserved.
doi:10.1016/j.cma.2010.10.014

having relatively smooth solutions; certainly, problems with solutions having jump discontinuities are not treated.

This paper is the first to systematically study, in the peridynamics setting, many algorithmic and implementation issues related to finite element methods, and especially discontinuous Galerkin methods. For this reason and for the sake of keeping the exposition simple, we only consider the *bond-based peridynamics* model [24] which treats only central forces between material points. However, more general peridynamics models have been developed. In [24], a preliminary version of the *state-based peridynamics* is introduced that allows one to consider shear forces. Then, in [30], the peridynamics state-based model is fully developed through the introduction of the notion of a non-ordinary peridynamic material so that the interaction between two points is not collinear with the line between the two points. See also [26] and especially the review paper [30]. The algorithms introduced in this paper can be extended to peridynamics states in a fairly straightforward manner.

In Section 2, we provide a short overview of bond-based peridynamics models including, in Section 2.2, the specific linearized peridynamics model for proportional microelastic materials. In Section 3, we first provide a variational formulation of the one-dimensional, linear peridynamics model. Then, we introduce the three finite element discretization methods used in our computational studies; these are based on continuous piecewise-linear, discontinuous piecewise-constant, and discontinuous piecewise-linear finite element spaces. That section also includes a brief discussion of theoretical error estimates. In Section 4, we list the data and exact solutions for the two one-dimensional problems we use to test the accuracy of the discretization methods we develop. One of these problems has a polynomial solution so it is representative of problems having smooth solutions whereas the second problem has a solution containing a jump discontinuity. The results of computational experiments are found in Sections 5–7. In these sections, we compare the relative advantages and disadvantages of the three methods and study their convergence behaviors. A particular focus of our studies is the effects that different choices for the horizon, a parameter that appears in the definition of the model, have on the accuracy of the resulting approximations. In Section 5 results for smooth solutions are given whereas, in Section 6, discontinuous exact solutions are considered for the case of having a grid point located exactly at the point where a jump discontinuity in the exact solution occurs. In Section 6, we also consider a hybrid method that combines discontinuous basis functions near the discontinuity with continuous basis functions away from the discontinuity. In Section 7, we again consider discontinuous exact solutions but in the more general situation of not having grid points coinciding with points of discontinuity of the exact solution. Ultimately, we develop a locally refined method that, when using discontinuous piecewise-linear finite element approximations, results in the same accuracy for nearly the same cost for problems having discontinuous solutions as it does for smooth solutions. In Section 8, we provide concluding remarks describing current and future work.

## 2. The peridynamics model

### 2.1. The general bond-based model

We follow the presentation of [24], the paper which introduced the peridynamics model. The equation of motion at any point $\mathbf{x}$ in the reference configuration at time $t$ is given by

$$\rho\ddot{\mathbf{u}}(\mathbf{x},t) = \int_{H_{\mathbf{x}}} \mathbf{f}(\mathbf{u}(\mathbf{x}',t)-\mathbf{u}(\mathbf{x},t),\mathbf{x}'-\mathbf{x})\mathrm{d}V_{\mathbf{x}'} + \mathbf{b}(\mathbf{x},t), \tag{1}$$

where $H_{\mathbf{x}}$ denotes a neighborhood of $\mathbf{x}$, $\mathbf{u}$ the displacement vector field, $\mathbf{b}$ a prescribed body force density field, $\rho$ the mass density in the reference configuration, and $\mathbf{f}$ a pairwise function whose value is the force density per unit volume that the particle located at $\mathbf{x}'$ (in the reference configuration) exerts on the particle located at the point $\mathbf{x}$ (also in the reference configuration). The relative position $\xi$ of these two particles in the reference configuration is given by $\xi = \mathbf{x}' - \mathbf{x}$ and their relative displacement $\boldsymbol{\eta}$ by $\boldsymbol{\eta} = \mathbf{u}(\mathbf{x}',t) - \mathbf{u}(\mathbf{x},t)$. Note that $\boldsymbol{\eta}+\xi$ is the relative position vector between the two particles in the deformed (or current) configuration.

The interaction between the particles located at $\mathbf{x}$ and $\mathbf{x}'$ is called a *bond*. The concept of a bond that extends over a finite distance is a fundamental difference between the peridynamic model and classical models for materials which are based on the idea of contact forces, i.e., interactions between particles that are in direct contact with each other.

Although interactions are nonlocal, we do assume that they are short ranged in the following sense. We assume that, for a given material, there exists a positive number $\delta$, called the *horizon*, such that

$$\mathbf{f}(\boldsymbol{\eta},\xi) = 0 \quad \forall\boldsymbol{\eta} \quad \text{whenever } |\xi| > \delta,$$

which means that the particle $\mathbf{x}$ cannot "see" beyond this horizon. We let $H_{\mathbf{x}}$ denote the spherical neighborhood of $\mathbf{x}$ in the body $R$ with radius $\delta$; see Fig. 1.

The pairwise force function $\mathbf{f}$ is required to have the following properties:

$$\mathbf{f}(-\boldsymbol{\eta},-\xi) = -\mathbf{f}(\boldsymbol{\eta},\xi), \quad \forall\boldsymbol{\eta},\xi, \tag{2}$$

which assures conservation of linear momentum and

$$(\xi+\boldsymbol{\eta})\times\mathbf{f}(\boldsymbol{\eta},\xi) = 0, \quad \forall\boldsymbol{\eta},\xi,$$

which assures conservation of angular momentum. The latter equation means that the force vector between two particles is parallel to their current relative position vector.

### 2.2. A linearized peridynamics model for microelastic materials

A material is said to be microelastic if the pairwise force function is derivable from a scalar micropotential $w$:

$$\mathbf{f}(\boldsymbol{\eta},\xi) = \frac{\partial w}{\partial\boldsymbol{\eta}}(\boldsymbol{\eta},\xi) \quad \forall\boldsymbol{\eta},\xi.$$

The micropotential is the energy in a single bond and has dimensions of energy per unit volume squared. The energy per unit volume in the body at a given point is therefore given by

$$W = \frac{1}{2}\int_{H_{\mathbf{x}}} w(\boldsymbol{\eta},\xi)\mathrm{d}V_{\xi}.$$

The factor 1/2 appears because each endpoint of a bond "owns" only half the energy in the bond.

If a body is composed of a *microelastic* material, the work done on it by external forces is stored in a recoverable form in much the same way as in classical theories of elasticity. Furthermore, it can be shown that the micropotential depends on the relative displacement vector $\boldsymbol{\eta}$ only through the scalar distance between the deformed points. Thus, there exists a scalar-valued function $\hat{w}$ such that

$$\hat{w}(y,\xi) = w(\boldsymbol{\eta},\xi), \quad \forall\boldsymbol{\eta},\xi, \qquad y = |\boldsymbol{\eta}+\xi|.$$

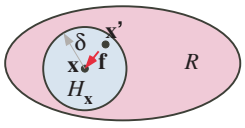


**Fig. 1.** Each point $\mathbf{x}$ in the body interacts, through bonds, directly with points $\mathbf{x}'$ in the sphere $H_{\mathbf{x}}$ having radius $\delta$.

Therefore, the interaction between any two points in a microelastic material may be thought of as an elastic (and possibly nonlinear) spring. The spring properties may depend on the separation vector $\xi$ in the reference configuration.

A *linearized* version of the peridynamic model for a microelastic material takes the form

$$\mathbf{f}(\boldsymbol{\eta},\xi) = \mathbf{C}(\xi)\boldsymbol{\eta}, \quad \forall \boldsymbol{\eta},\xi, \tag{3}$$

where $\mathbf{C}$, the micromodulus function for the material, is a second-order tensor given by

$$\mathbf{C}(\xi) = \frac{\partial \mathbf{f}}{\partial \boldsymbol{\eta}}(0,\xi), \quad \forall \xi. \tag{4}$$

This function inherits the following requirement from (2):

$$\mathbf{C}(-\xi) = \mathbf{C}(\xi) \quad \forall \xi. \tag{5}$$

For the special case of *proportional* materials [10,12,24], it follows from (3)–(5) that

$$\mathbf{C}(\xi) = c\frac{\boldsymbol{\xi}\otimes\boldsymbol{\xi}}{|\boldsymbol{\xi}|^3}, \quad \text{i.e.,} \quad C_{ij}(\xi) = c\frac{\xi_i\xi_j}{(\xi_k\xi_k)^{\frac{3}{2}}}, \tag{6}$$

where the latter expression uses components in a Cartesian coordinate frame and where $c$ denotes a constant that depends not only on the material, but also on the space dimension. For example, in one dimension, $c = 18k/5\delta^2$, where $k$ denotes the bulk modulus. The determination of $c$ is discussed in detail in [11] and the properties of $\mathbf{C}$ are discussed in [24].

Combining (1), (3), and (6), the linearized peridynamic model for a proportional, microelastic material is given by the integro-differential equation

$$\rho\ddot{\mathbf{u}}(\mathbf{x},t) = \int_{H_{\mathbf{x}}} c\frac{(\mathbf{x}'-\mathbf{x})\otimes(\mathbf{x}'-\mathbf{x})}{|\mathbf{x}'-\mathbf{x}|^3}(\mathbf{u}(\mathbf{x}',t)-\mathbf{u}(\mathbf{x},t))\mathrm{d}V_{\mathbf{x}'} + \mathbf{b}(\mathbf{x},t). \tag{7}$$

In this paper, we consider the steady-state, one-dimensional model setting for which (7), along with a "boundary" condition, reduces to[1]

$$\begin{cases} \frac{1}{\delta^2}\int_{x-\delta}^{x+\delta}\frac{u(x)-u(x')}{|x-x'|}\mathrm{d}x' = b(x), & x\in\Omega, \\ u(x) = g(x), & x\in\Gamma, \end{cases} \tag{8}$$

where, for convenience, we have set $\rho = 1$ and $k = 5/18$ and where[2]

$$\Omega = (\alpha,\beta), \quad \Omega' = (\alpha-\delta,\beta+\delta),$$
$$\Gamma = \overline{\Omega'}\setminus\Omega = [\alpha-\delta,\alpha]\cup[\beta,\beta+\delta].$$

## 3. Galerkin finite element discretizations

Let $S(\Omega')$ denote a Banach space[3] such that $S(\Omega')\subset L^2(\Omega')$. Define the affine space $S_g(\Omega') = \{u(x)\in S(\Omega') | u(x) = g(x) \text{ a.e. on } \Gamma\}$ and the subspace $S_0 = \{v(x)\in S(\Omega') | v(x) = 0 \text{ on } \Gamma\}$. We then pose the Galerkin variational problem

$$\begin{cases} \text{given } b(x)\in L^2(\Omega) \quad \text{and} \quad g(x)\in L^2(\Gamma), \\ \text{seek } u(x)\in S_g(\Omega') \text{ satisfying} \\ \frac{1}{\delta^2}\int_\alpha^\beta v(x)\int_{x-\delta}^{x+\delta}\frac{u(x)-u(x')}{|x-x'|}\mathrm{d}x'\,\mathrm{d}x \\ \qquad = \int_\alpha^\beta b(x)v(x)\mathrm{d}x, \quad \forall v(x)\in S_0(\Omega'), \end{cases} \tag{9}$$

corresponding to (8). The well-posedness of the variational problem (9) is shown in [16] for more general kernels, and for related problems, in [9,38]; see Section 3.4.

Let $S^h\subset S(\Omega')$ denote a family of finite-dimensional subspaces parameterized by a parameter $h$ which, in our setting, is a measure of the grid size. For $x\in\Gamma$, let $g^h(x)$ denote an approximation of $g(x)$; if $g(x)$ is sufficiently smooth, we can choose $g^h(x)\in S^h|_\Gamma$ to be an interpolant of $g(x)$; otherwise, we can choose $g^h(x)\in S^h|_\Gamma$ to be the $L^2(\Gamma)$ projection of $g(x)$. We then define the affine space $S_g^h = \{u^h(x)\in S^h | u^h(x) = g^h(x) \text{ a.e. on } \Gamma\}$ and the subspace $S_0^h = \{v^h\in S^h | v^h = 0 \text{ on } \Gamma\}\subset S_0(\Omega')$. Then, the Galerkin approximation to (9) is given by

$$\begin{cases} \text{given } b(x)\in L^2(\Omega) \quad \text{and} \quad g^h(x)\in S^h|_\Gamma, \\ \text{seek } u^h(x)\in S_g^h \text{ satisfying} \\ \frac{1}{\delta^2}\int_\alpha^\beta v^h(x)\int_{x-\delta}^{x+\delta}\frac{u^h(x)-u^h(x')}{|x-x'|}\mathrm{d}x'\,\mathrm{d}x \\ \qquad = \int_\alpha^\beta b(x)v^h(x)\mathrm{d}x, \quad \forall\ v^h(x)\in S_0^h. \end{cases} \tag{10}$$

Define a partition of $\Omega' = [\alpha-\delta,\beta+\delta]$ such that $x = \alpha-\delta$, $\alpha$, $\beta$, and $\beta+\delta$ are all nodes of the partition, i.e., we have, for given positive integers $K_1$, $K_2$, and $N$

$$\begin{aligned} \alpha-\delta = x_{-K_1} < \cdots < x_{-1} < \alpha = x_0 < x_1 < \cdots < x_N < x_{N+1} \\ = \beta < x_{N+2} < \cdots < x_{N+K_2+1} = \beta+\delta. \end{aligned} \tag{11}$$

Then, $h$ denotes the maximum length of any of the subintervals $(x_j,x_{j+1})$, $j = -K_1,\ldots,N+K_2$.

### 3.1. Continuous piecewise-linear finite element spaces

Choose $S^h$ to be the space of continuous piecewise-linear polynomials defined with respect to the partition (11). We also choose the standard "hat" functions $\{\phi_j(x)\}_{j=-K_1}^{N+K_2+1}$ as a basis for $S^h$.

Let $u^h(x) = \sum_{j=-K_1}^{N+K_2+1}u_j\phi_j(x)$ and, for $i = 1,\ldots,N$, let $v^h(x) = \phi_i(x)$. Then, (10) is equivalent to

$$\begin{aligned} &\frac{1}{\delta^2}\sum_{j=-K}^{N+K+1}u_j\int_\alpha^\beta\phi_i(x)\int_{x-\delta}^{x+\delta}\frac{\phi_j(x)-\phi_j(x')}{|x-x'|}\mathrm{d}x'\,\mathrm{d}x \\ &= \int_\alpha^\beta b(x)\phi_i(x)\mathrm{d}x, \end{aligned} \tag{12}$$

for $i = 1,\ldots,N$, where $u_j = g^h(x_j)$ for $j = -K_1,\ldots,0$ and $j = N+1,\ldots,N+K_2+1$. Because $g^h(x)$ is determined (by interpolation or projection) from the "boundary" data $g(x)$, these coefficients are determined from that data.[4]

Let the entries of the $N\times N$ matrix $\mathbb{A}$ be defined, for $i,j = 1,\ldots,N$, by

$$\mathbb{A}_{ij} = \frac{1}{\delta^2}\int_\alpha^\beta\phi_i(x)\int_{x-\delta}^{x+\delta}\frac{\phi_j(x)-\phi_j(x')}{|x-x'|}\mathrm{d}x'\,\mathrm{d}x \tag{13}$$

and let the components of the $N$-vector $\mathbf{b}$ be defined, for $i = 1,\ldots,N$, by

[1] In applying Eqs. (3)–(6) to arrive at Eqs. (7) and (8), we have assumed a specific constitutive relation. There are, of course, other constitutive choices, even in the linearized setting. For example, in [6,32], several other choices are considered in the one-dimensional setting.

[2] The second equation in (8) plays a role analogous to that of a Dirichlet boundary condition in classical elasticity, i.e., it fixes the displacement at the "boundary." For nonlocal models such as the one we consider, "boundary" data must be a priori specified on regions having nonzero volume and not just on lower-dimensional surfaces; see, e.g., [24]. This is needed for the well posedness of the "boundary-value" problem [16]. In one dimension, that data must be specified on intervals of size $\delta$, the peridynamics horizon. Thus, in the setting of Eq. (8), "boundary conditions" entail specifying "boundary" data on $\Gamma$, i.e., on the intervals $[\alpha-\delta,\alpha]$ and $[\beta,\beta+\delta]$, as part of the problem definition.

[3] In Section 3.4, we provide information about the specific solution space for (8).

[4] In particular, if it is possible to use the $S^h|_\Gamma$ interpolant, we have $u_j = g(x_j)$ for the indicated values of $j$.

$$\mathbf{b}_i = \int_\alpha^\beta b(x)\phi_i(x)\,dx - \sum_{j=-K}^{0} g^h(x_j)\int_\alpha^\beta \phi_i(x)\int_{x-\delta}^{x+\delta} \times \frac{\phi_j(x)-\phi_j(x')}{|x-x'|}\,dx'\,dx - \sum_{j=N+1}^{N+K+1} g^h(x_j)\int_\alpha^\beta \phi_i(x)\int_{x-\delta}^{x+\delta} \times \frac{\phi_j(x)-\phi_j(x')}{|x-x'|}\,dx'\,dx. \tag{14}$$

Also, let the entries of the $N$-vector $\mathbf{U}$ of unknown coefficients be defined by $\mathbf{U}_j = u_j$ for $j = 1,\ldots,N$. Then, the linear system (12) can be expressed in the form

$$\mathbb{A}\mathbf{U} = \mathbf{b}. \tag{15}$$

From the discussion in Section 3.4, it follows that the matrix $\mathbb{A}$ is symmetric and positive definite so that the linear system (15), or equivalently (12), has an unique solution which implies that the finite element approximation $u^h(x)$ determined from (10) is uniquely defined.

Due to the nonlocality of the peridynamic model, the matrix $\mathbb{A}$ is, in general, not tridiagonal, even though the basis functions are the piecewise linear hat functions. The right-hand side of (13) is a double integral, i.e., we have, for $i, j = 1,\ldots,N$

$$\mathbb{A}_{ij} = \frac{1}{\delta^2}\int_{x_{i-1}}^{x_{i+1}} \phi_i(x)\int_{x-\delta}^{x+\delta} \frac{\phi_j(x)-\phi_j(x')}{|x-x'|}\,dx'\,dx, \tag{16}$$

where we have used the fact that the basis function $\phi_i(x)$ has support confined to the interval $(x_{i-1},x_{i+1})$, i.e., $\phi_i(x) = 0$ whenever $x \notin (x_{i-1},x_{i+1})$. We also have that

$$\int_{x-\delta}^{x+\delta} \frac{\phi_j(x')}{|x-x'|}\,dx' \neq 0, \quad \text{whenever } \operatorname{supp}\{\phi_j(x')\} \in (x-\delta, x+\delta).$$

Suppose the partition (11) is uniform so that $K_1 = K_2 = K$ and $x_j = jh$ for $j = -K,\ldots,N+K+1$ and suppose $h < \delta$. Then, we have that $(x_j,x_{j+1}) \subset (x-\delta,x+\delta)$ so that for $j = i+2$ and perhaps for larger $j$, we have that $\mathbb{A}_{ij} \neq 0$ and likewise for $j = i-2$ and perhaps for smaller $j$. For example, if we choose $h$ such that $\delta = Mh$ for a fixed integer $M$, we have that

$$\mathbb{A}_{ij} = 0, \quad \text{if } j > i+M+1 \quad \text{or} \quad j < i-M-1$$

and $\mathbb{A}_{ij} \neq 0$ otherwise so that $\mathbb{A}$ is a banded matrix with fixed upper and lower half-bandwidth $M+1$. Note that the half-bandwidths increase as $h$ decreases. For example, if we choose a sequence of decreasing grid spacings $h = \delta/M$ with $M$ now an increasing sequence of integers, then the half-bandwidths increase linearly with $M$.[5]

In general, both the inner and outer integrals in (16) have to be approximated by quadrature rules.[6] If one applies a quadrature rule defined with respect to the interval $(x-\delta,x+\delta)$ to the inner integral, it is possible, because of the denominator $|x-x'|$, that the integrand is singular at one of the quadrature points. To guarantee that this does not occur, the outer integral is split into two integrals, one over each element, and then the inner integral can be split into several integrals in such a way that the possibility of the integrand being singular can be avoided. One can then safely apply Gauss quadrature rules to approximate each of the several outer and inner integrals.

### 3.2. Discontinuous piecewise-constant finite element spaces

The peridynamic model does not contain spatial derivatives of the solution so that finite element spaces consisting of functions with jump discontinuities are *conforming* for the variational formulation of the peridynamic model. Thus, we also consider such discontinuous finite element spaces for obtaining approximate solutions of the peridynamic model.

We again use the partition of $\Omega'$ defined in (11). Then, the simplest choice of basis functions for discontinuous Galerkin methods are the piecewise constants, i.e.:

$$\phi_j(x) = \begin{cases} 1, & \text{for } x \in (x_{j-1},x_j), \\ 0, & \text{otherwise}, \end{cases}$$

for $j = -K_1+1,\ldots,N+K_2+1$. Through the same process as for continuous piecewise linear functions, we are led to a linear system of the type (15), where now $\mathbb{A}$ is an $(N+1)\times(N+1)$ matrix and $\mathbf{U}$ and $\mathbf{b}$ are $(N+1)$-vectors. The diagonal entries of the matrix $\mathbb{A}$ are now given, for $i = 1,\ldots,N+1$, by

$$\begin{aligned}\delta^2\mathbb{A}_{ii} &= \int_{x_{i-1}}^{x_i}\int_{x-\delta}^{x+\delta} \frac{\phi_i(x)-\phi_i(x')}{|x-x'|}\,dx'\,dx \\ &= \int_{x_{i-1}}^{x_i}\int_{x-\delta}^{x+\delta} \frac{1}{|x-x'|}\,dx'\,dx - \int_{x_{i-1}}^{x_i}\int_{\max}^{(x_{i-1},x-\delta)\min(x_i,x+\delta)} \times \frac{1}{|x-x'|}\,dx'\,dx,\end{aligned} \tag{17}$$

where we have used the fact that $\phi_i(x) = 1$ within its support interval $(x_{i-1},x_i)$ and vanishes elsewhere. The off-diagonal entries are given by, as long as $\max(x_{j-1},x-\delta) < \min(x_j,x+\delta)$

$$\delta^2\mathbb{A}_{ij} = -\int_{x_{i-1}}^{x_i}\int_{\max}^{(x_{j-1},x-\delta)\min(x_j,x+\delta)} \frac{1}{|x-x'|}\,dx'\,dx, \tag{18}$$

for $i, j = 1,\ldots,N+1$, $j \neq i$, where we have also used the facts that $\phi_j(x) = 0$ for $x \in (x_{i-1},x_i)$ when $j \neq i$ and that $\phi_j(x') = 1$ within its support interval $(x_{j-1},x_j)$ and vanishes elsewhere. If $\max(x_{j-1},x-\delta) \geqslant \min(x_j,x+\delta)$, we have that $\mathbb{A}_{ij} = 0$. Clearly, $\mathbb{A}$ is a banded matrix and again, if $\delta$ is fixed independent of $h$, the bandwidth increases as $h$ is decreases, whereas, if $\delta$ is a multiple of $h$, the bandwidth remains fixed as $h$ is decreases.

An important observation about discontinuous Galerkin methods for the peridynamic model considered in this paper[7] is that, unlike the case for the application of such methods to elliptic partial differential equation problems, *there is no need to include "jump" terms that explicitly account for the continuity of fluxes across element boundaries.* Of course, this is a result of the fact that discontinuous finite element spaces are conforming for the variational formulation (9) of the peridynamic model.

### 3.3. Discontinuous piecewise-linear finite element spaces

Once again we use the partition of $\Omega'$ defined in (11). A basis for the space of discontinuous piecewise-linear discontinuous basis function is given by

$$\phi_{2j}(x) = \begin{cases} \frac{x_j - x}{x_j - x_{j-1}}, & \text{for } x \in (x_{j-1},x_j), \\ 0, & \text{otherwise} \end{cases}$$

[5] The horizon $\delta$ should be viewed as material parameter whose value is independent of the grid size $h$. However, in practice, it is often the case that $\delta$ is chosen proportional to $h$ so that $\delta$ decreases as $h$ decreases. In fact, such a strategy is even suggested in [24], the paper that introduced peridynamics, where the choice $\delta = 3h$ is recommended. One advantage of such a choice is that the bandwidth of the matrix $\mathbb{A}$ remains fixed as $h$ decreases. An important objective of our computational experimentation is to examine the effects that choosing $\delta$ proportional to $h$ has on the convergence and accuracy of approximate solutions and, in particular, to show that such a choice can lead to problems.

[6] For the computational experiments reported on in Sections 5–7, we use high-order quadrature rules so that quadrature errors do not affect the accuracy of the finite element approximations. However, for horizons that are small with respect to the grid size, we have observed some sensitivity in the accuracy with respect to the choice of quadrature rule so that this is an issue that deserves further study.

[7] For peridynamic models involving more singular kernels that result in smoother solutions, it is possible that jump terms may be needed.

and

$$\phi_{2j+1}(x) = \begin{cases} \frac{x-x_{j-1}}{x_j-x_{j-1}}, & \text{for } x \in (x_{j-1}, x_j), \\ 0, & \text{otherwise}, \end{cases}$$

for $j = -K_1 + 1, \ldots, K_2 + N + 1$. Now $\mathbb{A}$ is an $(2N+2) \times (2N+2)$ matrix and $\mathbf{U}$ and $\mathbf{b}$ are $(2N+2)$-vectors. For the sake of brevity, we do not write down formulas for the entries of the matrix $\mathbb{A}$.

An important observation is that *the space of* discontinuous *piecewise-linear functions contains the space of* continuous *piecewise-linear functions*. Obviously, the same cannot be said for the space of discontinuous piecewise-constant functions.

### 3.4. Theoretical convergence behavior

In [16], it is shown that the bilinear form[8]

$$A(u,v) = \frac{1}{\delta^2} \int_\alpha^\beta v(x) \int_{x-\delta}^{x+\delta} \frac{u(x) - u(x')}{|x - x'|} \, dx' \, dx, \tag{19}$$

associated with the variational problem (9) defines a norm on $S_0$; see also [9,38]. Further, results found in [38][9] indicate that, in two or more dimensions, that norm is equivalent to the $L^2(\Omega)$ norm. This is not the case in one dimension, the case considered in our computational studies. However, in [38], the one-dimensional case is also considered so that we can summarize what the results of that paper indicate about the finite element approximations defined in Sections 3.1,3.2,3.3 applied to the particular peridynamic variational problem (9).

Let the exact solution $u \in H^s(\Omega')$ for $s > 0$ and let

$$r = \begin{cases} \min\{1, s\} \\ \quad \text{for piecewice-constant finite element spaces}, \\ \min\{2, s\} \\ \quad \text{for piecewice-linear finite element spaces}, \end{cases} \tag{20}$$

where the second case applies to both continuous and discontinuous piecewice-linear finite element spaces. Then, from[10] [38], we have, with $C$ independent of $h$ and $\delta$

$$\|u - u^h\|_{L^2(\Omega')} \leqslant C h^{r-\gamma} \delta^{-1+\gamma} \|u\|_{H^s(\Omega')}, \tag{21}$$

for any $0 < \gamma < 1$. For fixed $\delta$, we see that, by choosing[11] $0 < \gamma = \epsilon \ll 1$, that the error estimate (21) implies that, with $C_\delta = O(\delta^{-1+\epsilon})$

$$\|u - u^h\|_{L^2(\Omega')} \leqslant C_\delta h^{r-\epsilon} \|u\|_{H^s(\Omega')}. \tag{22}$$

Note that the estimate (22) is not uniform in $\delta$. For $\delta =$ a constant multiple of $h$, we have, with $C$ independent of $h$ and $\delta$

$$\|u - u^h\|_{L^2(\Omega')} \leqslant C h^{r-1} \|u\|_{H^s(\Omega')}. \tag{23}$$

Note that for fixed $h$, (21) indicates that the approximate solution may diverge as $\delta \to 0$.

The fixed $\delta$ estimate (22) is nearly optimal[12] with respect to the convergence rate in $h$ because the error in the best approximation to a function $u \in H^s(\Omega')$ if of $O(h^r)$, i.e., (22) misses by an arbitrarily small reduction in the exponent. On the other hand, the estimate (23) for the case of $\delta$ being proportional to $h$ is suboptimal, i.e., the exponent is one less than that for the best approximation.

Additional discussions concerning theoretical error estimates are provided in Sections 6.1.3 and 7.

## 4. Model problems used in the computational experiments

For the computational experiments, we choose $\alpha = 0$ and $\beta = 1$ so that $\Omega = (0,1)$ and $\Omega' = (-\delta, 1+\delta)$.

We use the method of manufactured solutions to define problems for which the exact solutions are known. In some cases, this construction is facilitated by the following observations. If we assume that $u(x)$ is sufficiently smooth and apply Taylor's theorem to the left-hand side of (8), we obtain

$$\frac{1}{\delta^2} \int_{x-\delta}^{x+\delta} \frac{u(x) - u(x')}{|x - x'|} \, dx' = -\frac{1}{2} u''(x) - \frac{1}{48} u''''(x) \delta^2 + \cdots \tag{24}$$

which we can use to determine the right-hand side $b(x)$ of (8) for polynomial exact solutions $u(x)$. For example, from (24)

$$\text{for} \quad u(x) = x(1-x), \quad \text{we have } b(x) = 1. \tag{25}$$

The exact solution given in (25) is smooth and, of course, it is important to test a discretization method for the peridynamic model for such solutions. However, we also want to test discretization methods for problems with discontinuous solutions because one of the strengths of the peridynamic model is that it does not involve spatial derivatives so that is allows for solutions with jump discontinuities. Thus, we also test discretization methods for the exact solution

$$u(x) = \begin{cases} x, & \text{for } x < 0.5, \\ x^2, & \text{for } x > 0.5, \end{cases} \tag{26}$$

shown in Fig. 2 (left). Of course, we cannot use (24) to determine the corresponding right-hand side $b(x)$, so, by direct substitution, we determine it to be

$$b(x) = \begin{cases} 0, & \text{for } x \in I_1, \\ -\frac{1}{\delta^2}\left[\frac{1}{2}\delta^2 - \delta + \frac{3}{8} + \left(2\delta - \frac{3}{2} - \ln\delta\right)x \right. \\ \quad \left. + \left(\frac{3}{2} + \ln\delta\right)x^2 - (x^2 - x)\ln\left(\frac{1}{2} - x\right)\right], & \text{for } x \in I_2, \\ -\frac{1}{\delta^2}\left[\frac{1}{2}\delta^2 - \delta - \frac{3}{8} + \left(2\delta + \frac{3}{2} + \ln\delta\right)x \right. \\ \quad \left. - \left(\frac{3}{2} + \ln\delta\right)x^2 + (x^2 - x)\ln\left(x - \frac{1}{2}\right)\right], & \text{for } x \in I_3, \\ -1, & \text{for } x \in I_4, \end{cases}$$

where $I_1 = [0, 0.5 - \delta)$, $I_2 = [0.5 - \delta, 0.5)$, $I_3 = (0.5, 0.5 + \delta)$, and $I_4 = [0.5 + \delta, 1.0]$. For $\delta = 0.3$, a plot of this function is given in Fig. 2 (right).

[8] Actually, [16] considers a more general situation that includes Eq. (19) as a special case.

[9] The nonlocal "boundary conditions" considered in [38] are of a different type than those considered in this paper. In particular, the types of "boundary condition" treated in [38] allow the use of Fourier transforms which facilitates the analysis and numerical analysis. Thus, the results of [38] do not strictly apply to the model treated here, but, nonetheless, one can expect similar results. We note that several interesting results about the dependence on $h$ and $\delta$ of the condition number of the coefficient matrix $\mathbb{A}$ of the discretized system are also given in [38].

[10] The error estimates Eqs. (21)–(23) quoted from [38] were derived for worst case scenarios and were applicable for more general solutions than those considered here. The solutions described in Section 4 are either a low-order polynomial or a piecewise low-order polynomial. Moreover, these solutions are independent of the model parameter $\delta$. In general, one expects that $b$ is a given quantity independent of $\delta$, but the exact and numerical solutions may both depend on $\delta$ implicitly, especially when their high-frequency components have sensitive dependence on $\delta$. In such cases, the dependence of the error on $\delta$ could be more subtle and some sensitivity might be observed.

[11] Note that we cannot choose $\epsilon = 0$; this is one effect of the fact that the norm defined by the bilinear form is not equivalent to the $L^2(\Omega')$ norm.

[12] We say that an approximation of a given function, including functions defined as a solution of classical or nonlocal boundary-value problems, as being *optimally accurate* or *converging at an optimal rate* if the rate of convergence with respect to the grid size $h$ is the same as that of the best approximation out of the same approximating space. Note that, in the finite element setting, the rate of convergence of a best approximation depends on the smoothness of the function being approximated, the degree of the polynomials used, the norm used to measure the error, and properties of the grid; in one dimension, an example of a grid property is the locations of the grid points relative to the points of discontinuity of the solution.

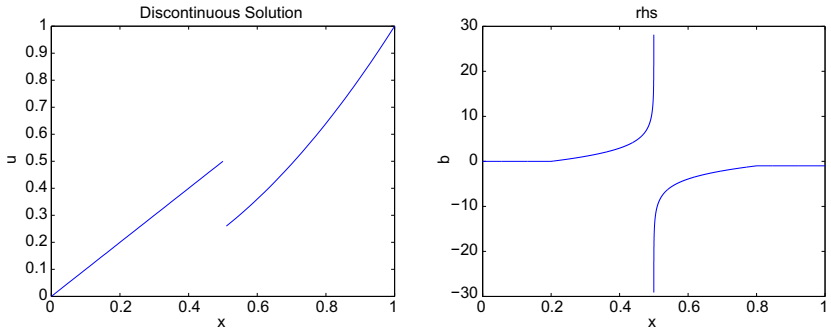


**Fig. 2.** Left: the discontinuous solution (26), right: the corresponding forcing function $b(x)$.

## 5. Computational results for smooth solutions

We present results of computational experiments for the model problems having the smooth solution (25) and for each of the three discretization schemes discussed in Sections 3.1–3.3. In the tables and figures, we provide the $L^2(\Omega)$ and $L^\infty(\Omega)$ norms and, where appropriate, the $H^1(\Omega)$ semi-norms of the error and the corresponding rates of convergence for a sequence of grid sizes. We also examine two choices for how the horizon $\delta$ is related to the grid size $h$. We take the view that the horizon is a material parameter so that its value is independent of the grid size. Recall that, in this case, the bandwidth of the coefficient matrix $\mathbb{A}$ increases as $h$ decreases. Also note that because the peridynamics model is a continuum one, it makes sense to choose $h$ smaller than $\delta$ and to in fact, discuss the behavior of approximate solutions as[13] $h \to 0$. We also examine the case suggested in [24] for which the horizon is chosen proportional to the grid size in order to ascertain if there exist problems for which such a choice produces meaningful approximations.[14]

We begin with the *continuous piecewise-linear finite element* discretization discussed in Section 3.1. Specifically, for the smooth exact solution given in (25), we present, in Fig. 3 (top), results for $\delta = 2h$, $3h$, and $4h$, i.e., the horizon is chosen to be proportional to the grid size. In Fig. 3 (bottom), we present results for $\delta = 0.1$, 0.01, and 0.001, i.e., the horizon is chosen independent of the grid size; note that $h < \delta$ for some values of $h$ and $h > \delta$ for others. From this figure, we make the following observations:

- For smooth solutions such as the one given in (25), continuous piecewise-linear finite element approximations of the linear peridynamic model (8) converge at the optimal rates, i.e., the $L^2$ and $L^\infty$ errors are roughly of $O(h^2)$ and the $H^1$ errors are roughly of $O(h)$. This statement is true both if the horizon $\delta$ is chosen proportional to the grid size $h$ or if it is chosen fixed independent of $h$. In the case for which $\delta$ is fixed, optimal convergence rates are attained for both $\delta < h$ and $\delta > h$. There also seems to be almost no discernible effect on the convergence behavior with respect to $h$ as $\delta$ decreases.
- For smooth solutions, the rates of convergence attained by continuous piecewise-linear finite element approximations of the linear peridynamic model are the same as those obtained from the analogous finite element discretization of linear classical elastic models.

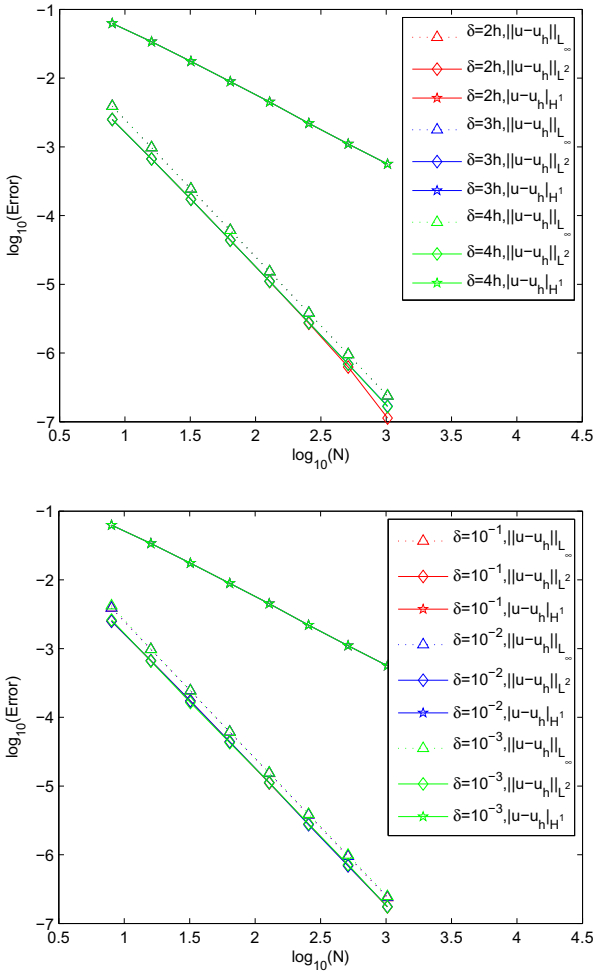


**Fig. 3.** $L^2$, $L^\infty$, and $H^1$ errors vs. $N = 1/h$ for continuous piecewise linear approximations for the smooth exact solution (25); top: for $\delta = 2h$, $3h$, and $4h$; bottom: for $\delta = 0.1$, 0.01, and 0.001.

We next consider the *discontinuous piecewise-constant and piecewise-linear finite element* discretizations discussed in Sections 3.2 and 3.3, respectively. Recall that, unlike for second-order elliptic partial differential equations, such finite element spaces are conforming for the peridynamic model. Figs. 4 and 5 provide results for the piecewise-constant and piecewise-linear cases, respectively.

For the piecewise-constant case, we provide results for both $\delta$ proportional to $h$ and $\delta$ independent of $h$ whereas for the piece-

[13] This is in contrast to discrete models such as molecular dynamics for which the inter-particle spacing is a material parameter so that the interaction radius cannot be smaller than that spacing.

[14] In [6], similar computational experiments were carried out for a particle-like discretization of Eq. (8) effected by applying a quadrature rule directly to the integral appearing in that equation. That paper also considered two other kernel functions in addition to that of Eq. (8). For smooth solutions, the results reported on here are consistent with those of [6]. We note that solutions with jump discontinuities were not considered in [6].

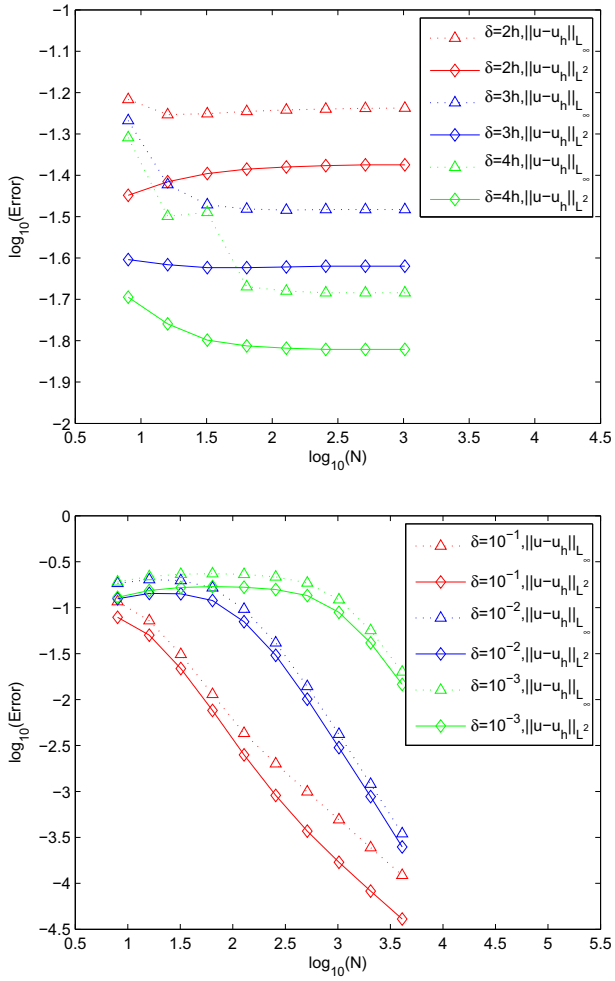


**Fig. 4.** $L^2$ and $L^\infty$ errors vs. $N = 1/h$ for discontinuous piecewise-constant approximations for the smooth exact solution (25); top: for $\delta = 2h$, $3h$, and $4h$; bottom: for $\delta = 0.1$, 0.01, and 0.001.

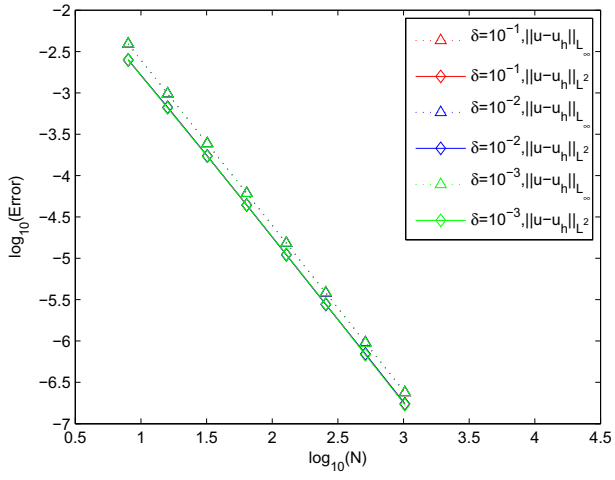


**Fig. 5.** $L^2$ and $L^\infty$ errors vs. $N = 1/h$ for discontinuous piecewise-linear approximations for $\delta = 0.1$, 0.01, and 0.001 for the smooth exact solution (25).

wise-linear case, only the $\delta$ independent of $h$ case is considered. From these figures, we make the following observations.

- If the horizon $\delta$ is chosen proportional to the grid size $h$, piecewise-constant approximations fail to converge for smooth exact solutions.
- On the other hand, if $\delta$ is fixed independent of $h$, piecewise-constant approximations converge optimally for smooth solutions, e.g., the $L^2$ and $L^\infty$ errors are roughly of $O(h)$, provided $h$ is sufficiently small relative to $\delta$. Seemingly, one needs $h < \delta$.
- If $\delta$ is fixed independent of $h$, discontinuous piecewise-linear approximations converge at optimal rates for smooth solutions, e.g., the $L^2$ and $L^\infty$ errors are roughly of $O(h^2)$. Optimal convergence rates are attained for both $\delta < h$ and $\delta > h$.

### 5.1. Discussion of results for smooth solutions

We draw several conclusions from the computational results presented in Figs. 3–5, as well the results of other computational experiments not reported on here. Of course, many more computational studies and numerical analyses are needed, especially in two and three dimensions and for nonlinear problems, before these conclusions and those in other sections can be made more definitive.

#### 5.1.1. Continuous and discontinuous piecewise-linear discretizations

We compare the results provided in Figs. 3 and 5 with the theoretical predictions given by the error estimates (22) and (23). Note that because the solution is smooth, we have that $r = 2$ in those estimates. With respect to the convergence with respect to the grid size $h$, the computational results for the $L^2$ norm of the error are in agreement with the theoretical error estimate (22) for $\delta$ independent of $h$ which predicts that the error is of $O(h^2)$. Of course, we do not have any theoretical error estimates with respect to the $L^\infty$ norm and $H^1$ semi-norm; however, the computational results indicate that the finite element approximations are roughly optimal for those norms as well. On the other hand, for the case of $\delta$ proportional to $h$, the computational results indicate a better convergence rate than that predicted by the estimate (23). Of course, this is not a contradiction because the error estimates only provide an upper bound on the error; however, many more computational experiments are needed before one can conclude that the error estimate (23) is not sharp.

With respect to the dependence of the error on the horizon $\delta$, the computational results for continuous and discontinuous piecewise-linear discretizations do not show the growth indicated by the error estimate (21). In fact, both Figs. 3 and 5 show a lack of sensitivity of the $L^2$, $L^\infty$, and $H^1$ errors with respect to $\delta$ as is evidenced by the fact that the plots for different values of $\delta$ lie on top of each other.

The fact that, for smooth solutions, optimally accurate approximations are obtained even for $\delta < h$ is noteworthy. For such $\delta$, the peridynamic model essentially becomes a local model so that smooth solutions are basically obtainable from a local model. Thus, for such solutions, one may well be able to use classical elastic models involving partial differential equations. From the accuracy point of view, there also seems to be little advantage, relative to classical elastic models, to using the peridynammics model for problems with smooth solutions. Another interpretation of the fact that, for smooth solutions, optimally accurate solutions are obtained for any choice of $\delta$ is that, in such a case, $\delta$ should not be interpreted as being a material parameter and thus can be chosen for convenience, e.g., to minimize bandwidth or to simplify the coupling of the continuum peridynamic model to atomistic models.

The observation that discontinuous piecewise-linear approximations lead to optimally accurate results for smooth solutions is not surprising, given that they are conforming for the peridynamic model and that they contain as a subspace the continuous piece-

wise-linear functions, i.e., discontinuous piecewise-linear approximations must be at least as good as continuous piecewise-linear approximations. As was the case for continuous piecewise linear approximations, optimally accurate solutions are obtained for any choice of $\delta$ so that again, $\delta$ can be interpreted as being a parameter and that can be chosen for convenience.

In summary, the computational results indicate that both continuous and discontinuous piecewise-linear discretizations are safe to use within the peridynamic framework for problems having smooth solutions.

*5.1.2. Discontinuous piecewise-constant discretizations*

The results provided in Fig. 4 for discontinuous piecewise-constant discretizations indicate that, if $\delta$ is chosen proportional to $h$, approximations fail to converge; in fact, the error is independent of $h$. Because for the piecewise-constant discretization $r = 1$, this is in agreement with the prediction of (23). If $\delta$ is chosen independent of $h$, optimal rates are seemingly obtained only if $h < \delta$; this restriction can be problematic in practice. In addition, we now do see that, for fixed $h$, the error grows as $\delta$ decreases which is in agreement with the prediction of (21).

In summary, the computational results indicate that discontinuous piecewise-constant discretizations are not robust, even for smooth solutions.

## 6. Computational results for discontinuous solutions with grid points coinciding with points of discontinuity

In this section, computational results are presented for the discontinuous exact solution (26) for the "best-case scenario" in which a *grid point is placed exactly at the location of the point at which the jump discontinuity occurs.*[15] The main reason we use this "best-case scenario" is to compare the different finite element methods we study in a setting for which the accuracy is not compromised by having the discontinuity occur inside an element. We again consider the three discretization schemes discussed in Sections 3.1–3.3.

Fig. 6 provides results for the *continuous piecewise-linear finite element* discretization discussed in Section 3.1. Errors with respect to the $H^1$-semi norm are not provided because the exact solution does not belong to $H^1(\Omega)$. From this figure, we make the following observations.

- For solutions containing jump discontinuities such as the one given in (26), continuous piecewise-linear finite element approximations of the linear peridynamic model (8) are seriously compromised, even though we place a grid point exactly at the point of discontinuity of the exact solution. The $L^2$ errors are of $O(h^{1/2})$ and there is no convergence with respect to the $L^\infty$ norm. This statement is true both if the horizon $\delta$ is chosen proportional to the grid size $h$ or if it is chosen fixed independent of $h$.

For the *discontinuous piecewise-constant finite element* discretization described in Section 3.2, Fig. 7 provides results for the case for which the horizon $\delta$ is chosen proportional to the grid size $h$ and in, Fig. 7, results are provided for the case for which the horizon is chosen independent of the grid size. Results for the *discontinuous piecewise-linear finite element* discretization described in Section 3.3 are given in Fig. 8 for the case of $\delta$ chosen independent of $h$. From these figures, we make the following observations.

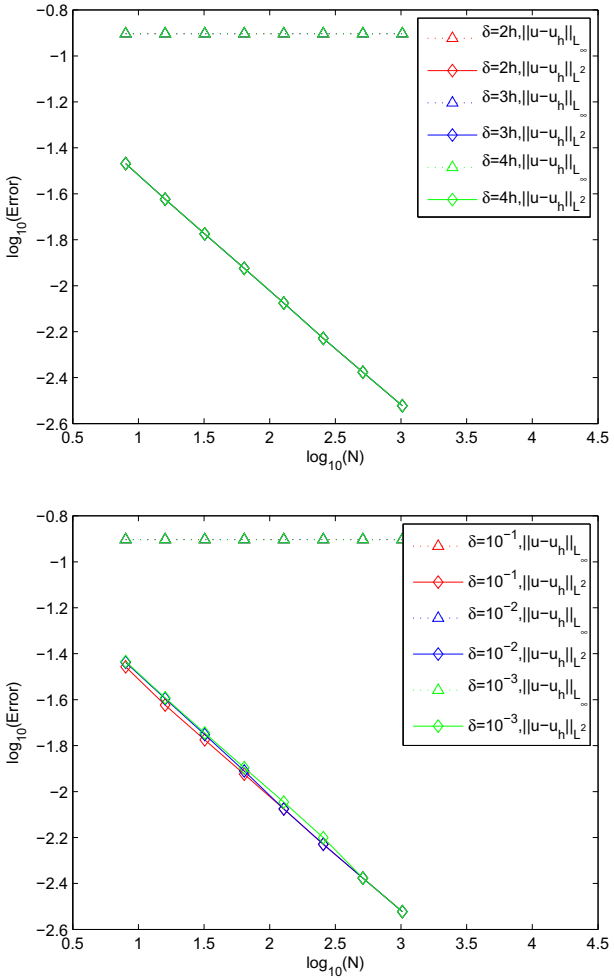


**Fig. 6.** $L^2$ and $L^\infty$ errors vs. $N = 1/h$ for continuous piecewise linear approximations for the discontinuous exact solution (26); top: for $\delta = 2h$, $3h$, and $4h$; bottom: for $\delta = 0.1$, $0.01$, and $0.001$.

- As was the case for smooth solutions, if the horizon $\delta$ is chosen proportional to the grid size $h$, piecewise-constant approximations fail to converge for solutions that contain a jump discontinuity, even if a grid point is placed at the point of discontinuity.
- For solutions that contain a jump discontinuity and if $\delta$ is fixed independent of $h$, piecewise-constant approximations converge at the same rates as that obtained for smooth solutions, provided $h$ is sufficiently small relative to $\delta$ and provided a grid point is placed at the point of discontinuity. Seemingly, one needs $h < \delta$.
- For solutions that contain a jump discontinuity, if $\delta$ is fixed independent of $h$, discontinuous piecewise-linear approximations converge at the same rates as that obtained for smooth solutions, if a grid point is placed at the point of discontinuity.

*6.1. Discussion for discontinuous solutions with grid points coinciding with the points of discontinuity*

We draw several conclusions from the computational results presented in Figs. 6–8, as well the results of other computational experiments not reported on here.

*6.1.1. Continuous piecewise-linear discretizations*

The results provided in Fig. 6 indicate that the best one can hope for is approximately $O(h^{1/2})$ accuracy with respect to the $L^2$ norms

[15] In Section 7, we discuss what happens when points of discontinuity do not coincide with grid points.

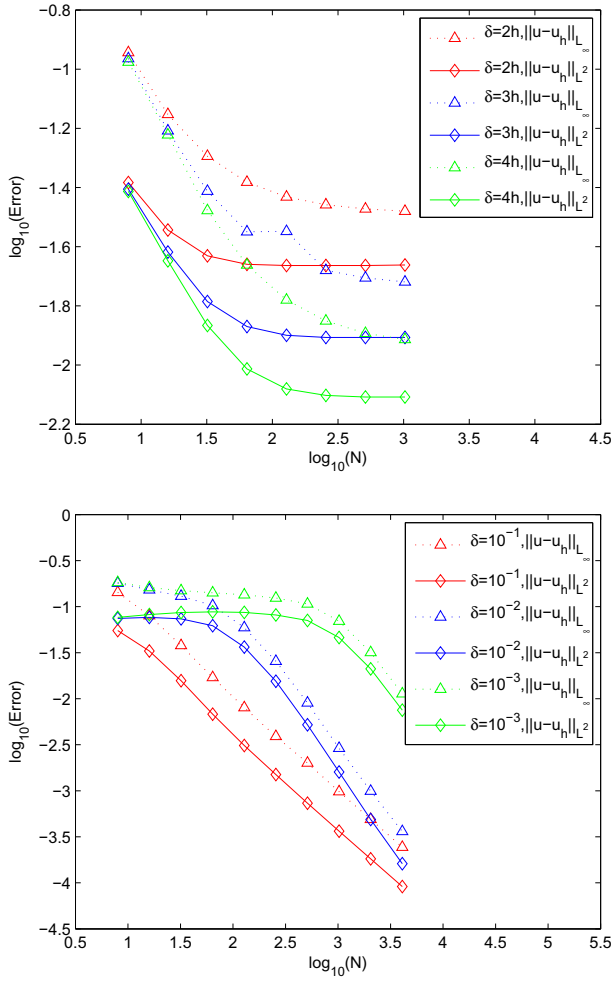


**Fig. 7.** $L^2$ and $L^\infty$ errors vs. $N = 1/h$ for discontinuous piecewise-constant approximations for the discontinuous exact solution (26); top: for $\delta = 2h$, $3h$, and $4h$; bottom: for $\delta = 0.1$, 0.01, and 0.001.

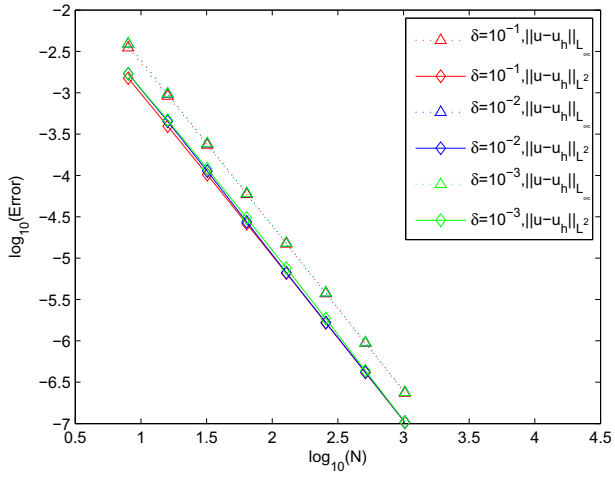


**Fig. 8.** $L^2$ and $L^\infty$ errors vs. $N = 1/h$ for discontinuous piecewise-linear approximations for the discontinuous exact solution (26) for $\delta = 0.1$, 0.01, and 0.001.

obtained when the horizon is chosen independent of the grid size. According to (22), this $L^2$ rate of convergence is optimal, given that the exact solution belongs to $H^{1/2-\theta}(\Omega)$ for any $\theta > 0$ but is no smoother than that, i.e., we have $s = 1/2 - \theta$ so that $r \approx 1/2$ in (22). The lack of convergence with respect to the $L^\infty$ norm is also expected, given that the best continuous piecewise-linear approximation with respect to that norm behaves in the same way. Note that, as was the case for smooth exact solutions, one does not observe the sensitivity of the error with respect to $\delta$ predicted by (21). Note also that these results cannot be improved by increasing the degree of the polynomials used and that analogous finite element discretization of linear classical elastic models would yield similar results.

In summary, the results indicate that continuous piecewise-linear finite element approximations are practically useless for problems with solutions containing jump discontinuities, even if a grid point is placed at the location of the jump discontinuity of the exact solution.

### 6.1.2. Discontinuous piecewise-constant discretizations

The results provided in Fig. 7 indicate that *discontinuous piecewise-constant* finite element approximations are not robust for problems having jump discontinuities, even if a grid point is placed at the location of the jump discontinuity of the exact solution. This is not surprising, given that, in Section 5, such discretizations were also found to be not robust for problems having smooth solutions. Again, if the horizon is chosen to be proportional to the grid size, no convergence is obtained whereas, if the horizon is chosen to be independent of the grid size, $O(h)$ convergence is achieved, provided that $h < \delta$. Note that, as was the case for smooth exact solutions, one does now observe the sensitivity of the error with respect to $\delta$ predicted by (21).

The $L^2$ rates of convergence given in Fig. 7, at least for $h < \delta$, are better than predicted by (22), given that, for the exact solution (26), we have $r \approx 1/2$. The $L^\infty$ rates of convergence are also better than one would expect, given what was expected for the $L^2$ rates. Why the computed rates are better is discussed in Section 6.1.3.

### 6.1.3. Discontinuous piecewise-linear discretizations

The results provided in Fig. 8 indicate that, if a grid point is placed at the location of the jump discontinuity of the exact solution, one obtains the same $L^2$ and $L^\infty$ rates of convergence with respect to the grid size $h$ as those obtained for smooth solutions. As was the case for piecewise-constant discretizations, these $L^2$ rates of convergence are better than predicted by (22), given that, for the exact solution (26), we still have $r \approx 1/2$. Note that here one does not observe the sensitivity of the error with respect to $\delta$ predicted by (21).

Why are the $L^2$ rates of convergence with respect to the grid size $h$ better than predicted by the results of Section 3.4? First, recall that error estimates such as those given in Section 3.4 are a combination two estimates. First, we have a standard finite element estimate of the type

$$\|u - u^h\|_{L^2(\Omega')} \leqslant C_\theta \inf_{v^h \in S^h} \|u - v^h\|_{L^2(\Omega')}, \tag{27}$$

where, in our situation, $C_\theta = C_\delta h^{-\theta}$ for any $\theta > 0$ due to the non-equivalence of the norm induced by the bilinear form in (19) and the $L^2(\Omega)$ norm.[16] Second, we use results from approximation theory to estimate the error in the best approximation appearing on the right-hand side of (27). In obtaining the error estimates in Section 3.4, one assumes that the exact solution belongs to $H^s(\Omega')$ for which approximation theory combined with (27) yields the estimates given in that section. No notice is made in Section 3.4 of the possibility of the exact solution being *piecewise smooth*, as is the case for the exact solution (26).

[16] In two and higher dimensions, $C_\theta$ is independent of $\theta$. Note that, in general, $C_\theta$ depends on $\delta$.

For *continuous* finite element spaces, one cannot take advantage of the piecewise smoothness of the exact solution, even if grid points are placed at the points of discontinuity of the solution. Thus, the estimates given in Section 3.4 are sharp, as is evidenced by the results given in Fig. 6.

The situation for *discontinuous* finite element spaces is very different. Suppose that, in the one-dimensional setting we consider here, we have one point at which a jump discontinuity in the exact solution $u$ occurs.[17] Let $\Omega_1$ and $\Omega_2$ denote the domains on each side of the jump discontinuity and assume that a grid point is located at the point at which the jump discontinuity occurs, i.e., at the interface point between $\Omega_1$ and $\Omega_2$, Then, for discontinuous finite element spaces, we have that[18]

$$\inf_{v^h\in S^h}\|u-v^h\|_{L^2(\Omega')} = \inf_{v^h\in S^h|_{\Omega_1}}\|u-v^h\|_{L^2(\Omega_1)} + \inf_{v^h\in S^h|_{\Omega_2}}\|u - v^h\|_{L^2(\Omega_2)}, \tag{28}$$

where $S^h|_{\Omega_i}$ denotes the restriction of the functions in $S^h$ to $\Omega_i$. Then, e.g., the error estimate (22) is replaced with the estimate

$$\|u-u^h\|_{L^2(\Omega')} \leqslant C_\delta h^{r-\epsilon}\Big(\|u\|_{H^s(\Omega_1)} + \|u\|_{H^s(\Omega_2)}\Big). \tag{29}$$

Now, in each of $\Omega_1$ and $\Omega_2$, the exact solution is smooth so that we can choose $r = 1$ and 2 for discontinuous piecewise-constant and piecewise-linear approximations, respectively. The convergence rates (with respect to the grid size $h$) obtained from (29) for problems with a jump discontinuity are then the same as those obtained from (22) for smooth solutions. This is exactly what is observed in Figs. 7 and 8.

Error estimates such as (27) are not available for the $L^\infty$ norm so we cannot extend much of the above discussion to this setting. However, we do note that the best $L^\infty$ norm approximation for discontinuous finite element spaces satisfies a relation just like (28) and, from Fig. 8, we see that the Galerkin finite element solution has the same $L^\infty$ convergence rates for solutions with jump discontinuities as it did for smooth solutions, if a grid point is placed at the location of the jump discontinuity.

In summary, the results indicate that *discontinuous piecewise-linear* finite element approximations are very well suited for problems containing jump discontinuities, at least when grid points are placed at the locations of the jump discontinuities of the exact solution. The observation that discontinuous piecewise-linear approximations can lead to optimally accurate results for *discontinuous* solutions illustrates an important potential of peridynamic models: one can obtain accurate results for problems with discontinuities for which finite element methods for classical elastic models that involve derivatives cannot.

### 6.2. A hybrid continuous–discontinuous Galerkin method

From the results just presented, it is evident that discontinuous piecewise-linear finite element approximations result in better accuracy compared to either the continuous piecewise-linear or the discontinuous piecewise-constant approximations; see the summary in Table 1 for the exact solution given in (26). However, for the same number of finite element intervals, the discontinuous piecewise-linear method has greater complexity than the other two methods; again see Table 1. Which approach is better, with respect to accuracy per unit cost, between methods having greater accuracy and complexity and those having lesser accuracy and complexity depends on the number of space dimensions and the method selected for solving the linear systems. Certainly, in the one-dimensional setting and in case grid points are located at the points of discontinuity of the exact solution, an accuracy per cost analysis shows that the discontinuous piecewise-linear approximation wins out over the other two approximations.

**Table 1**
For the discontinuous exact solution (26), a comparison of the $L^2$ rates of convergence and matrix properties for continuous-linear (CL), discontinuous-constant (DC), and discontinuous-linear (DL) finite element approximations for $h = 1/(N+1)$ and $\delta = Mh$, where $N$ and $M$ are positive integers; the number of degrees of freedom and the half bandwidth of the coefficient matrix. The dimension of that matrix, i.e., the number or rows and columns, is, of course, equal to the degrees of freedom.

| | CL | DC | DL |
|---|---|---|---|
| $L^2$ errors | $O(N^{-1/2})$ | $O(N^{-1})$ | $O(N^{-2})$ |
| Degrees of freedom | $N$ | $N+1$ | $2N+2$ |
| Half bandwidth | $M+1$ | $M$ | $2M+1$ |

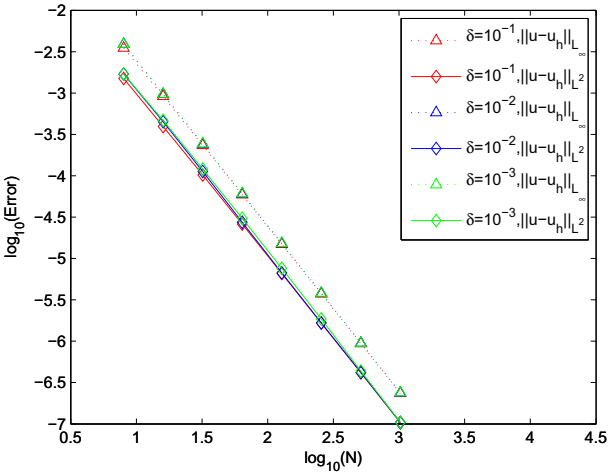


**Fig. 9.** $L^2$ and $L^\infty$ errors vs. $N = 1/h$ for hybrid discontinuous/continuous piecewise-linear approximations for the discontinuous exact solution (26) for $\delta = 0.1$, 0.01, and 0.001.

In Section 5, we saw that, for smooth exact solutions such as that given by (25), continuous and discontinuous piecewise-linear approximations result in the same convergence behavior. This observation offers the possibility of using continuous piecewise-linear approximations for smooth parts of a solution having jump discontinuities and using discontinuous piecewise-linear approximations only in "small" neighborhoods of each jump discontinuity; at this stage, we are still requiring that a gird point is placed at the location of each jump discontinuity. In such a situation, the error estimate (29) holds so that one should be able to preserve the high accuracy of the discontinuous piecewise-linear approximations for solutions having jump discontinuities, but with a complexity very near that of continuous piecewise-linear approximations. We illustrate this idea for the *discontinuous* exact solution (26); the results are given in Fig. 9. Discontinuous basis functions are used only in one interval on each side of the point of discontinuity. We see that even though we use continuous approximations almost everywhere, the hybrid approximation results in the same rates of convergence as if we use discontinuous approximations everywhere, provided a grid point is located at the point of discontinuity of the exact solution. Note that this is achieved without any need for grid refinement.

[17] Obviously, a finite number of jump discontinuities can be handled in an analogous manner.

[18] Such a division in the best approximation error does not hold for continuous finite element spaces.

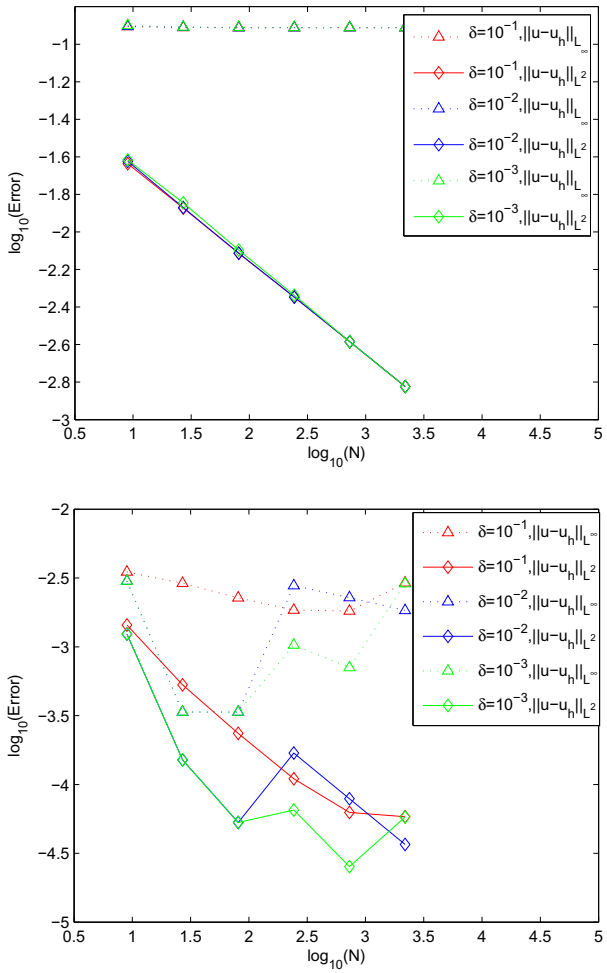


**Fig. 10.** $L^2$ and $L^\infty$ errors vs. $N = 1/h$ for discontinuous piecewise-linear approximations for the discontinuous exact solution (26) for the case in which there is no grid point located at the jump discontinuity of the solution. Top: errors calculated using all intervals; bottom: errors calculated by omitting the interval containing the jump discontinuity.

## 7. Computational results for discontinuous solutions with grid points not coinciding with points of discontinuity

We have shown that finite element discretizations of the peridynamic model for materials has the potential of producing accurate solutions, even for discontinuous solutions. In particular, discontinuous piecewise-linear approximations are apparently robustly optimally accurate with respect to choices for the model parameter, i.e., the horizon $\delta$, and the smoothness of the solution, so long as one places a grid point at any point at which a jump discontinuity of the exact solution occurs. Of course, to take advantage of this, one has to know where the jump discontinuities occur so that one would have to implement some type of method to detect the appearance of discontinuities. In two and higher dimensions, even if this was possible, i.e., if one could exactly locate the surfaces across which discontinuities occur, one would still not be able to recover the full accuracy possible with discontinuous piecewise-linear approximations as was possible in Section 6. The reason for this is that if the surfaces of discontinuity are curved, one cannot, in general, have grid cell faces exactly align with those surfaces.

The top plot of Fig. 10 gives an indication of what can happen if one does not place a grid point at the location of the jump discontinuity of the solution; the exact solution is still given by (26), but for all levels of refinement, no grid point falls at the point of discontinuity $x = 0.5$. We use the discontinuous piecewise-linear discretizations[19] that worked so well when a grid point is located at the point of discontinuity. However, now, the rate of convergence with respect to the $L^2$ norm deteriorates to 0.5; with respect to the $L^\infty$ norm, no convergence is achieved.[20]

Straightforward implementations of the finite element methods used in Section 5 that ignore the possible presence of discontinuities along with a straightforward interpretation of results that use global norms for the error are doomed to suffer the severe loss of accuracy just alluded to. This is because the best approximation suffers in exactly the same way, i.e., if the exact solution $u$ contains a jump discontinuity, we have, for any discontinuous finite element space $S^h$

$$\inf_{v^h \in S^h} \|u - v^h\|_{L^2(\Omega')} = O(h^{1/2}) \quad \text{and} \quad \inf_{v^h \in S^h} \|u - v^h\|_{L^\infty(\Omega')} = O(h^0).$$

These estimates hold regardless of the degree of polynomials used within the individual elements.

### 7.1. Identifying jump discontinuities in the solution

Clearly, from what we just saw, we cannot ignore the presence of jump discontinuities. However, if we are to develop approaches that, in some way, take into account such discontinuities, we must be able to identify their location, at least approximately. Fortunately, although in practice it is not usually possible to determine the exact location of surfaces of discontinuity of an exact solution, in the discontinuous Galerkin setting, it is possible to at least determine which elements those surfaces intersect.

For example, consider Fig. 11 from which one can clearly discern from the approximate solution that a discontinuity occurs in the interval $I_d$ containing the point $x = 0.5$ which is the location of the jump discontinuity of the exact solution. Thus, although we cannot discern from the approximate solution that a discontinuity occurs at exactly $x = 0.5$, we can discern that a discontinuity occurs within the interval containing that point.[21]

### 7.2. Failed attempts at recovering full accuracy

We now examine two natural approaches that, at first look, would seem take advantage of the fact that one can identify elements within which discontinuities occur, but in the end do not.

First, note that there are other interesting things about the plots in Fig. 11. Clearly one sees that the $L^\infty$ norm of the error does not decrease with decreasing grid sizes but also does not increase. We also see from Fig. 11 that there are no Gibbs oscillations associated with the approximate solutions. In fact, there seems to always be only two egregious values in the approximate solution and those occur at the left and right ends (the red cross and blue dot, respectively, that are far from the exact solution) of the interval $I_d$. This gross inaccuracy does not carry over to neighboring intervals; e.g., note that the red cross (the approximate solution at the left

[19] The computational results for discontinuous piecewise-constant basis functions are the same.

[20] Note, however, that unlike for discontinuous piecewise linear finite element approximations, continuous finite element approximations yields results similar to those in the top plot of Fig. 10 *even if a grid point is placed at a point of discontinuity*; see Fig. 6. The major difference between continuous and discontinuous bases are that the former belong to $H^1(\Omega)$ whereas the latter do not. As a result, approximating an exact solution that does not belong to $H^1(\Omega)$ causes additional problems for continuous finite element spaces that do not occur for discontinuous spaces.

[21] A perhaps more difficult situation is that for which the solution exhibits large gradients in localized regions as opposed to sharp discontinuities. However, although in the large gradient case the sharp discontinuity apparent in Fig. 11 is replaced by a smeared out discontinuity, one should be able to identify regions of sharp gradients and mitigate errors in such regions by grid refinement.

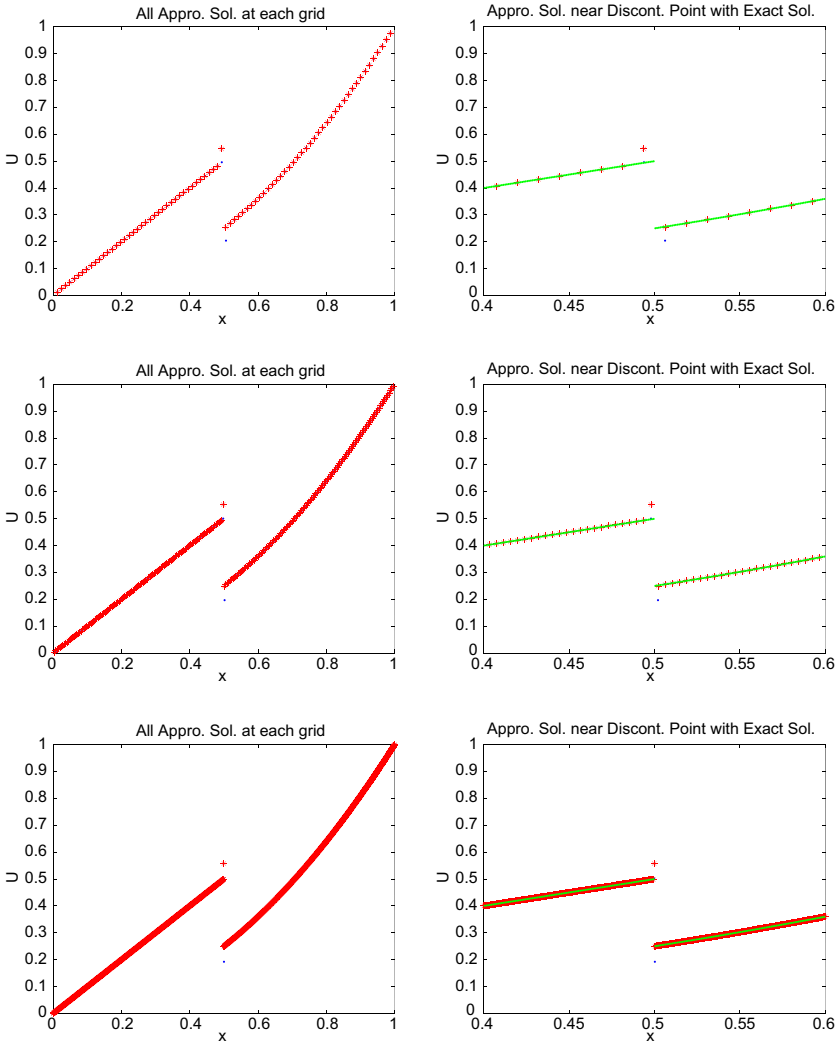


**Fig. 11.** Left column and top to bottom: discontinuous Galerkin piecewise-linear finite element approximation for the discontinuous exact solution (26) for $h = 3^{-4}$, $3^{-5}$, and $3^{-7}$ with $\delta = 0.01$; for all grids, the discontinuity in the exact solution is in the interior of a finite element. The red crosses and blue dots correspond to the solution at the right and left end of each finite element interval, respectively. Note that most of the blue dots are not visible because they are covered by the red crosses. Right column: a zoom in (near the point of discontinuity of the exact solution) of the corresponding approximate solutions in the left column superimposed on the exact solution (the solid green curve). (For interpretation of the references to colour in this figure legend, the reader is referred to the web version of this article.)

end point of interval to the right of $I_d$) at the same location as the egregious blue dot is much a more accurate approximation. The corresponding situation occurs to the left of $I_d$, with the roles of the blue dots and red crosses reversed.

At each grid point we have two choices for the value of the approximate solution. Then, given the observations of the previous paragraph, it is natural to choose the blue points to the left of the discontinuity and the red points to the right of the discontinuity, at least near the discontinuity. This certainly eliminates the egregious values noted above. Unfortunately, that is not enough; the loss of accuracy persists. In fact, for the top plot of Fig. 10, we have already done exactly that which is why the $L^\infty$ errors there are considerably smaller than the errors corresponding to the egregious values.

Fig. 11 suggests another approach towards the possible recovery of the full accuracy possible with discontinuous piecewise-linear discretizations, at least away from points of discontinuity. Let

$$\widetilde{\Omega}'_h = \Omega' \setminus \{\text{all intervals containing a point of discontinuity}\}.$$

We then only compute error norms with respect to $\widetilde{\Omega}'_h$, hoping that, by leaving out the intervals containing jump discontinuities in the solution, one obtain the same accuracy as that obtained for smooth solutions. The reason one is hopeful that this approach would work is that, as is shown in Section 7.3, this is what happens for both the $L^2$ and $L^\infty$ best approximations. Unfortunately, this does not imply that the discontinuous Galerkin approximations to the peridynamic model has the same behavior because, e.g., the $L^2\left(\widetilde{\Omega}'_h\right)$ norm of the error is not, in general, bounded by a multiple of the error in the best approximation measured in that norm. An indication that this is so is given by the results of the bottom plot of Fig. 10. Comparing the results of the two plots of Fig. 10 shows that outside the interval containing the discontinuity, the error is much smaller than within that interval. Certainly, however, we do not recover the full accuracy of the best approximation and, in fact, the errors are quite erratic. A contributor to the erratic behavior is that the error is affected by the distance from the point of discontinuity to the nearest grid point. Note that omitting from the error calculation a few more intervals in the neighborhood of the discontinuity in the exact solution improves the error somewhat, but does not completely cure the erratic behavior.

### 7.3. A local grid refinement approach that recovers full accuracy

We first note that the subdivision of the error in the best approximation into the sum of errors in the best approximations

over two intervals given in (28) can be extended to the sum over the finite elements. Specifically, let $\{E_j\}$, $\{h_j\}$, and $\{s_j\}$, respectively, denote the set of finite elements, their corresponding grid sizes, and the Sobolev smoothness index of the exact solution within the elements. Define $r_j$ as in (20) with $s$ replaced by $s_j$. We than have that

$$\inf_{v^h\in S^h}\|u-v^h\|_{L^2(\Omega')} = \sum_{E_j}\inf_{v^h\in S^h|_{E_j}}\|u-v^h\|_{L^2(E_j)} \leqslant C_\delta\sum_{E_j}h_j^{r_j-\epsilon}\|u|_{E_j}\|_{s_j}, \tag{30}$$

where $(\cdot)|_{E_j}$ denotes the restriction to the element $E_j$. For simplicity, we assume the simple one-dimensional setting for which the exact solution contains only a single jump discontinuity. Let $I_d$ denote the element which contains the jump discontinuity and let $h_d$ denotes its length. Assume that all the other elements have length $h$. In the element $I_d$, we have $r_j = 1/2-\theta$ whereas in all other elements we have $r_j = 1$ and 2 for piecewise-constant and piecewise-linear discretizations, respectively. Then, (30) implies that

$$\inf_{v^h\in S^h}\|u-v^h\|_{L^2(\Omega')} = O\left(h_d^{1/2-\theta}+h^{r-\theta}\right), \tag{31}$$

for any $\theta>0$, where, e.g., $r=1$ and 2 for discontinuous piecewise constant and piecewise linear approximations, respectively.[22] Then, if we choose[23] $h_d = h^{2r}$, we have that

$$\inf_{v^h\in S^h}\|u-v^h\|_{L^2(\Omega')} = O(h^{r-2\theta}), \tag{32}$$

i.e., with respect to the grid size used outside the intervals containing jump discontinuities in the exact solution, *the best approximation recovers the rate of convergence obtainable for smooth solutions.*

We still have that the $L^2(\Omega')$ norm of the error of discontinuous Galerkin finite element approximations is bounded by a constant multiple of the $L^2(\Omega')$ norm of the errors in the best approximations. Thus, the estimates (31) and (32) remain valid for discontinuous Galerkin finite element approximations. This is seen in the top plot in Fig. 12. These results are for discontinuous piecewise-liner approximations of the problem having exact solution (26); a constant grid size $h$ is used everywhere except for the single interval containing the jump discontinuity which has a grid size $h^4$. We see that the $L^2$ convergence rates are the same as for smooth solutions, even though the discontinuity in the exact solution occurs within an element.[24]

Note also the approach of locally refining the grid does not help at all with the $L^\infty$ norm of the error; this is to be expected because although the equality in (30) also holds for the $L^\infty$ norm, the error in the best $L^\infty$ approximation with respect to the interval that contains the jump discontinuity remains of $O(1)$ regardless how small the size of that interval. On the other hand, if we ignore that interval, the error in best $L^\infty$ approximation would be the same as for smooth solutions. Of course, because we do not have an estimate such as (27) for the $L^\infty$ norm, we have no reason to expect that the discontinuous piecewise-linear Galerkin finite element solution behaves in the same way; however, the results given in the bottom plot in Fig. 12 indicate that, surprisingly, it does.

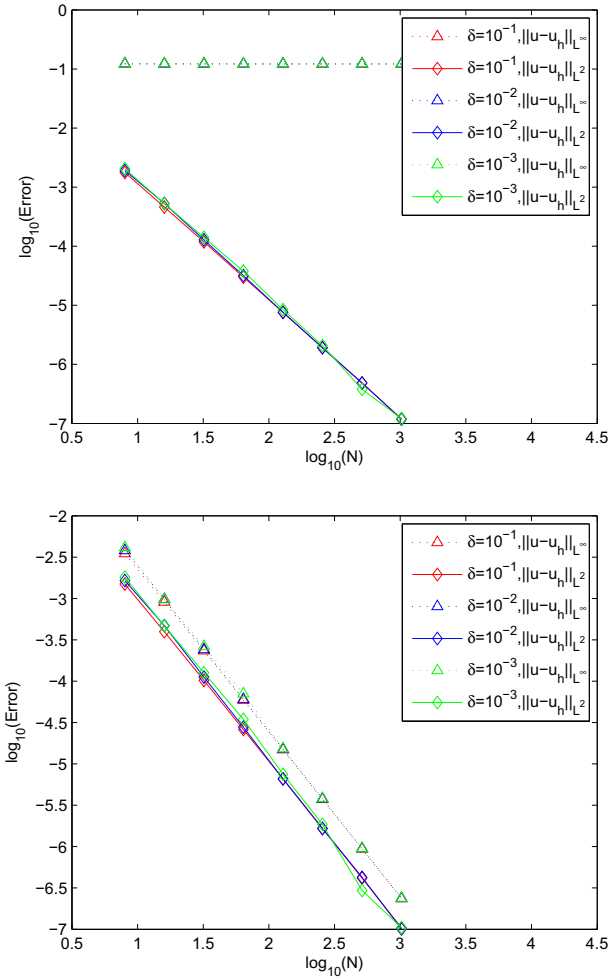


**Fig. 12.** $L^2$ and $L^\infty$ errors of discontinuous piecewise-linear approximations for the discontinuous exact solution (26) for the case in which there is no grid point located at the point of discontinuity of the solution. The interval containing the jump discontinuity has length $h^4$. Top: all intervals contribute to the error calculation. Bottom: the contribution to the error from the interval containing the jump discontinuity is ignored.

The results given here and the discussion of Section 7.1 lead to a possible *local* adaptive strategy for obtaining approximations of discontinuous solutions that converge at the same rates as for smooth solutions, even if the points of discontinuity occur within a finite element. In Section 7.1, we saw that, when using discontinuous finite element spaces, it is possible to identify the intervals at which jump discontinuities in the solution occur. An adaptive strategy could then be used to recursively refine those intervals until, for piecewise-linear approximations, the discontinuities are isolated within intervals of size $h^4$ relative to the grid size in the rest of the domain. Refined intervals that do not contain the discontinuity can be de-refined so that one ends up with very local refinement; in principle, only one refined interval is needed for each point of discontinuity. Note also that because we are using discontinuous finite element spaces, the grid size can changed abruptly from $h$ to $h^4$ and back, as it did for the results of Fig. 12. Note also that this refinement strategy can be extended to two and three dimensions where one would end up with a layer of elements following surfaces across which the exact solution has a jump discontinuity. With respect to the grid size away from the discontinuity, this adaptive strategy will yield the same $L^2$ convergence rates as that for smooth solutions. To effect the same recovery in the $L^\infty$ convergence rates one seemingly need only ignore

[22] The estimates (31) and (32) still involve constants that depend on the horizon $\delta$ but here we focus on convergence rates with respect to the grid size.

[23] For dimensional consistency, what we really mean here is that a constant grid size $h$ is used everywhere except for the single interval containing the jump discontinuity which has size $h_d = \ell(h/\ell)^{2r}$, where $\ell$is, e.g., the diameter of the material sample. Alternately, one can view our discussion to apply to non-dimensionalized models in which $\ell$is used to non-dimensionalize lengths.

[24] In [6], an adaptive refinement strategy is proposed and tested for problems having point loads that result in continuous solutions. That strategy resulted in refinement over several nodes as opposed to the local, single-element refinement discussed here.

the contributions to the errors emanating from the finite elements that intersect surfaces of discontinuity.

Much the same as discussed in Section 6.2, one can define a hybrid method for which discontinuous basis functions are used in the refined elements and continuous basis functions are used in the remaining elements.

## 8. Concluding remarks

Current and future work addresses implementations of the finite element methodology in two and three dimensions. Extension of the methodology to peridynamics state-based models and to nonlinear problems are also being considered. Of particular interest are adaptive grid refinement strategies for problems having solutions containing jump discontinuities. Given the estimates in [38], a related question of interest is the effects that local refinements have on the condition numbers of the resulting algebraic systems. Discontinuous approximations based on higher-degree polynomials are also of interest as is the study of effective quadrature rules for the assembly of the discrete systems. Complete, rigorous analyses of errors and convergence rates and of adaptive grid refinement strategies are also being pursued.

## Acknowledgements

The authors thank the referees for their careful reading of this paper and for their many suggestions that resulted in substantial improvements.

## References

[1] B. Altan, Uniqueness of initial-boundary value problems in nonlocal elasticity, Int. J. Solids Struct. 25 (1989) 1271–1278.
[2] B. Altan, Uniqueness in nonlocal thermoelasticity, J. Therm. Stresses 14 (1991) 121–128.
[3] Z. Bazant, M. Jirasek, Nonlocal integral formulations of plasticity and damage: survey and progress, J. Engrg. Mech. 128 (2002) 1119–1149.
[4] F. Bobaru, S. Silling, Peridynamic 3D problems of nanofiber networks and carbon nanotube-reinforced composites, in: Materials and Design: Proceedings of the International Conference on Numerical Methods in Industrial Forming Processes, American Institute of Physics, 2004, pp. 1565–1570.
[5] F. Bobaru, S. Silling, H. Jiang, Peridynamic fracture and damage modeling of membranes and nanofiber networks, in: Proceedings of the XI International Conference on Fracture, Turin, vol. 5748, 2005, pp. 1–6.
[6] F. Bobaru, M. Yang, L. Alves, S. Silling, E. Askari, J. Xu, Convergence, adaptive refinement, and scaling in 1D peridynamics, Int. J. Numer. Methods Engrg. 77 (2009) 852–877.
[7] Y. Chen, J. Lee, A. Eskandarian, Atomistic viewpoint of the applicability of microcontinuum theories, Int. J. Solids Struct. 41 (2004) 2085–2097.
[8] K. Dayal, K. Bhattacharya, Kinetics of phase transformations in the peridynamic formulation of continuum mechanics, J. Mech. Phys. Solids 54 (2006) 1811–1842.
[9] Q. Du, K. Zhou, Mathematical analysis for the peridynamic nonlocal continuum theory, Math. Model. Numer. Anal. (2010), doi:10.1051/m2an/2010040.
[10] E. Emmrich, O. Weckner, The peridynamic equation of motion in non-local elasticity theory, in: Proceedings of the III European Conference on Computational Mechanics Solids, Structures and Coupled Problems in Engineering, Lisbon, 2006.
[11] E. Emmrich, O. Weckner, Analysis and numerical approximation of an integrodifferential equation modelling non-local effects in linear elasticity, Math. Mech. Solids 12 (2007) 363–384.
[12] E. Emmrich, O. Weckner, On the well-posedness of the linear peridynamic model and its convergence towards the Navier equation of linear elasticity, Commun. Math. Sci. 5 (2007) 851–864.
[13] E. Emmrich, O. Weckner, The peridynamic equation and its spatial discretization, Math. Model. Anal. 12 (2007) 17–27.
[14] W. Gerstle, N. Sau, Peridynamic modeling of concrete structures, in: L. Li et al. (Eds.), Proceedings of the Fifth International Conference on Fracture Mechanics of Concrete Structures, vol. 2, Ia-FRAMCOS, 2004, pp. 949–956.
[15] W. Gerstle, N. Sau, S. Silling, Peridynamic modeling of plain and reinforced concrete structures, in: SMiRT18: 18th International Conference on Structural Mechanics in Reactor Technology, Beijing, 2005.
[16] M. Gunzburger, R. Lehoucq, A nonlocal vector calculus with application to nonlocal boundary value problems, Multiscale Model. Simul. 8 (2010) 1581–1598.
[17] E. Kroner, Elasticity theory of materials with long range forces, Int. J. Solids Struct. 3 (1967) 731–742.
[18] I. Kunin, Elastic Media with Microstructure, vols. I–II, Springer, Berlin, 1982/83.
[19] Y. Lei, M. Friswell, S. Adhikari, A Galerkin method for distributed systems with non-local damping, Int. J. Solids Struct. 42 (2005), doi:10.1016/j.ijsolstr.2005.06.058.
[20] R. Maceka, S. Silling, Peridynamics via finite element analysis, Finite Elem. Anal. Des. 4 (2007) 1169–1178.
[21] A. Pisano, P. Fuschi, Closed form solution for a nonlocal elastic bar in tension, Int. J. Solids Struct. 40 (2003) 13–23.
[22] C. Polizzotto, Nonlocal elasticity and related variational principles, Int. J. Solids Struct. 38 (2001) 7359–7380.
[23] D. Rogula, Nonlocal Theory of Material Media, Springer, Berlin, 1982.
[24] S. Silling, Reformulation of elasticity theory for discontinuities and long-range forces, J. Mech. Phys. Solids 48 (2000) 175–209.
[25] S. Silling, Dynamic fracture modeling with a meshfree peridynamic code, in: K. Bathe (Ed.), Computational Fluid and Solid Mechanics, Elsevier, Amsterdam, 2003, pp. 641–644.
[26] S. Silling, Linearized theory of peridynamic states, J. Elast. 99 (2010) 85–111.
[27] S. Silling, E. Askari, Peridynamic modeling of impact damage, in: F. Moody (Ed.), PVP, vol. 489, ASME, New York, 2004, pp. 197–205.
[28] S. Silling, E. Askari, A meshfree method based on the peridynamic model of solid mechanics, Comput. Struct. 83 (2005) 1526–1535.
[29] S. Silling, F. Bobaru, Peridynamic modeling of membranes and fibers, Int. J. Nonlinear Mech. 40 (2005) 395–409.
[30] S. Silling, M. Epton, O. Weckner, J. Xu, E. Askari, Peridynamic states and constitutive modeling, J. Elast. 88 (2007) 151–184.
[31] S. Silling, R. Lehoucq, Peridynamic theory of solid mechanics, Adv. Appl. Mech. 44 (2010) 73–168.
[32] S. Silling, M. Zimmermann, R. Abeyaratne, Deformation of a peridynamic bar, J. Elast. 73 (2003) 173–190.
[33] J. Wang, R. Dhaliwal, Uniqueness in generalized nonlocal thermoelasticity, J. Therm. Stresses 16 (1993) 71–77.
[34] J. Wang, R. Dhaliwal, On some theorems in the nonlocal theory of micropolar elasticity, Int. J. Solids Struct. 30 (1993) 1331–1338.
[35] O. Weckner, R. Abeyaratne, The effect of long-range forces on the dynamics of a bar, J. Mech. Phys. Solids 53 (2005) 705–728.
[36] O. Weckner, E. Emmrich, Numerical simulation of the dynamics of a nonlocal, inhomogeneous, infinite bar, J. Comput. Appl. Mech. 6 (2005) 311–319.
[37] O. Weckner, E. Emmrich, Energy conserving spatial discretisation methods for the peridynamic equation of motion in non-local elasticity theory, Preprint 25-2005, Institute of Mathematics, TU Berlin, 2005.
[38] K. Zhou, Q. Du, Mathematical and numerical analysis of linear peridynamic models with nonlocal boundary conditions, SIAM J. Numer. Anal. 48 (2010) 1759–1780.
[39] M. Zimmermann, A Continuum Theory with Long-Range Forces for Solids, Ph.D. Thesis, Department of Mechanical Engineering, Massachusetts Institute of Technology, 2005.